When AE (Acoustic Emission) meets AI (Artificial Intelligence)

Kilian WASMER[1], Fatemeh SAEIDI[1], Bastian MEYLAN[1], Farzad VAKILI-FARAHANI[1] and Sergey A. SHEVCHIK [1]
[1] Swiss Federal Laboratories for Materials Science and Technology (Empa), Thun, Switzerland

Contact e-mail: kilian.wasmer@empa.ch

Abstract. On the one hand, in recent years, artificial intelligence is a new trend that showed itself as a very powerful tool to overcome both the complexity and/or the large amount of data to be treated. On the other hand, acoustic emission has been proven to be an effective tool for monitoring and control in multiple processes. In this contribution, we presents three examples from completely different fields where acoustic emission technique is combined with artificial intelligence to make a significant step forward for process monitoring and quality control.

The first example shows the possibility to predict failure in lubricated surfaces using acoustic time-frequency features and random forest algorithm. Although scuffing is a stochastic failure mechanism, we can predict it 5 mins before it takes place. We proved this for a grey cast iron - hardened 42CrMo6 steel tribo-pair.

The second example depicts an *in situ* and real-time monitoring electrical discharge in solids, where the induced mechanical damage is estimated by acoustics.

The last example addresses the quality control in additive manufacturing and laser welding, which are at the centre of attention for years. We will show how acoustic emission combined with artificial intelligence can be used for differentiating the type of weld and detecting some type of defects.

Introduction

Acoustic Emission (AE) analysis is one of the most effective monitoring methods with high sensitivity and reliability in detection of changes in materials. Consequently, AE has been used successfully in many engineering applications and for a broad variety of materials, material compositions and structures [1]. The engineering applications include tribology [2], failure of components [3] and, more recently, laser welding and/or additive manufacturing [4, 5]. However, despite the technical simplicity in collecting of AE data, its processing is not a trivial task. The reason is that each specific application requires a specific interpretation of the acoustic signals in terms of the underlying physical phenomena. Artificial intelligence (AI) makes such interpretation by correlating the acquired AE with the real events. In real life conditions and industrial environment, the collected data is distinguished for intricate dependencies between inputs/outputs and the presence of intensive background noises. This is an inherent problem, especially in tribology, facture mechanics, laser welding and additive manufacturing.

In tribology and fracture mechanics, the AE signals during friction of solids can be generated by at least nine factors: (1) elastic interaction & impacts; (2) changes in stress-strain state of a local volume of slid surface layer; (3) plastic deformation and damage; (4) generation, motion and interaction of dislocation; (5) energy liberation at repeated deformation or phase hardening-weakening and damage of surface layer; (6) changes in friction surface structure; (7) formation of micro-cracks, micro-pores and new surfaces because of wear; (8) appearance of wear debris and (9) surface spalling and formation of fatigue pit [2].

Laser welding and additive manufacturing are similar in many aspects. In both processes, the content of AE includes the echoes from material changes, melt dynamics and solidification processes. The latter is distinguished by the formation of crack that also have unique acoustic signatures. This means that AE content is affected by the substrate characteristics (e.g. chemical constituents, surface quality, environments) and process parameters (e.g. laser type, spot size, laser power, scan speed, and scan line spacing). In addition, the AE is enriched by components, generated from the pores, balling, unfused materials, and cracking. All aforementioned factors are impossible to predict and the process dynamics is dependant from a large amount of parameters.

With all mentioned above, the relation between the AE content in relation and the real underlying physical event is of extreme complexity and is not always possible to do. In many cases, the solution requires very expensive equipment like synchrotron, where the necessary information is accessible *in situ* and in real-time. Unfortunately, such experiments are time-consuming, costly and with some limitations such as the sample size. The latter, despite getting a fundamental understanding of the AE event, the experimental results may not be transferable to real life conditions. The other investigation methods are based on a post-mortem analysis which always includes a certain level of uncertainties. AI methods allow bypassing these constraints by using high non-linear data transforms that allows reducing the effect of noises, complex data structure and even the non-accuracies in preparations of training sets.

Wavelet decomposition

The monitoring of the evolution of AE signals in time allows understanding the dynamics of the underlying process. Fast Fourier transform (FFT) spectrum [6] and Short-Time Fourier Transform (STFT) [7]-[8] are often used for such an analysis. Unfortunately, FFT is principally limited to stationary and time invariant signals and it does not retain the time domain information [6]. STFT [7]-[8] is intrinsically limited due to a resolution problem [6]. As an alternative approach and unlike the Fourier transform, the wavelet transform (WT) provides simultaneous description of a signal on both time and frequency domains [9]. WT can specify the frequency of the signals and the time associated to those frequencies.

According to the discrete wavelet transform (DWT) principle [6]-[10], at each decomposition level, part of the frequency components (starting from the maximum acquired frequency) is extracted from the original signal in a sequential order. The extracted parts are the so-called *details* whereas the remained signal is named *approximation*. The *approximation* signal can be further decomposed into a next level, so that the signal is broken down into lower frequency components [6]-[11]. Based on the theory of wavelet decomposition, the signal after *n*-th decomposition level is expressed as:

$$S = A_n + \sum_{i=1}^{n} D_i + \varepsilon \tag{1}$$

where S is the signal, A and D are the reconstructed *approximation* and *details*, respectively, while ε represents the approximation error which depends on the type of the mother wavelet (modulation function) used to decompose the signal. The decomposition tree at multiple levels for the given signal S is shown in Fig. 1 .

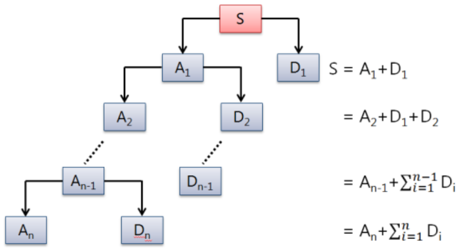

Fig. 1 Wavelet decomposition tree

Many families of wavelet exist (e.g. Daubechies, Symlet, Coiflets, BiorSplines, Meyer, Gaussian, Mexican hat, Morlet). In these works, the mother wavelet having the minimum error of the reconstructed signal in Eq. 1 was used. Apart from that, we use the data adaptive wavelets to minimize the approximation error if none from the standard wavelets provide with acceptable approximation accuracy. The same specialised wavelets are used here for detection of separate patterns within the signals.

1. Example: AE meets AI in the field of tribology

The example explained below was reported with details in [12]. In this work, an SRV reciprocating tribometer schematically illustrated in Fig. 2 was used. An environmental control unit helps to keep the test conditions in the chamber constant with a temperature of 35 °C and a relative humidity of 30%. The test configuration is flat-on-flat as it is known to be problematic and, therefore, a special holder was used to prevent the inclination of the counter-body and to ensure flat-on-flat conditions.

The counter-body (42CrMo4 steel) was oscillating with a stroke of 4 mm at a frequency of 6 Hz with an estimated sliding time of 54 ms for each stroke as seen from Fig. 3. A constant load of 600 N, giving a nominal pressure of 24 MPa, was applied on the contact surface. The coefficient of friction (COF), the sample temperature, the applied load and the stroke were continuously monitored and recorded by the tribometer software. The sampling rate was 16 ms for the COF and 2 s for the other parameters. A representative curve for one forward and back stroke taken from SRV tribometer software is illustrated in Fig. 3. Fig. 4 demonstrates how well the COF correlates with the AE RMS data.

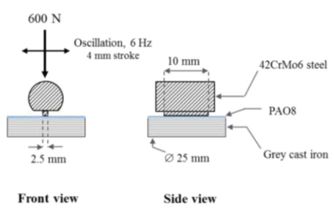

Fig. 2. Tribo-test set-up (a) Reciprocating tribometer (SRV® III), and (b) schematic diagram of the counter-body and the bottom sample

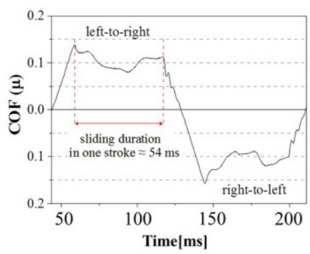

Fig. 3. Values of friction coefficients for one forward and back strokes

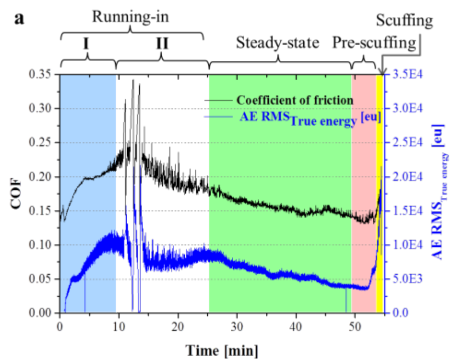

Fig. 4. Variation of the AE *RMS* and COF with time and the friction regimes: running-in, steady-state, pre-scuffing and scuffing

In order to achieve the starved lubrication conditions and consequently scuffing, the lubrication of the cast iron surface was performed by spraying a small quantity (0.4 μl/cm2) of pure poly-alpha-olefin oil (PAO) with a viscosity of 8 cSt using a high precision spraying machine. The weight of the sprayed oil was controlled by an accurate weighing (±0.1 mg).

On specific tribo-tests, an acoustic emission (AE) sensor was mounted close to the cast iron sample with a thin layer of grease and fixed with a paper tape. The signals were recorded using a Vallen acquisition system and a PAC WD sensor. The selected sensor has a broadband response range from 100 kHz to 1 MHz. The pre-amplifier had a fixed gain setting of 34 dB. The sampling rate was 1 MHz with a record duration of 65 ms to cover a complete stroke. To eliminate the noise from the tribometer, the best threshold was found at 29 dB. Fig. 5 shows a typical AE signal (waveform) collected by the AE system.

In the present work, all AE signals were decomposed with the wavelet packet transform using the Daubeshies wavelet with ten vanishing moments (known as db10 in Matlab 2012). Db10 showed to be the most suitable wavelet for the collected AE signals as it provides the minimum approximation errors for the collected signals.

The changes in the AE content were employed to describe the momentary surface modifications. The changes were extracted from two consecutive AE signals obtained from the current and the previous strokes. The entire dataset was processed using the following procedure: Each signal is decomposed and a set of WP is extracted using Daubeshies wavelet. The corresponding time-frequency content was then divided into separate non-overlapping frames (F). Each F is a two-dimensional structure that bounds a limited set of WP. This set is defined by the height (N) that corresponds to the number of scales j (see Eq. (1)) and a width (M) that corresponds to a fixed time span. The time span for different frames within the signal is adjusted to compensate the acceleration and deceleration of the counter-body relative to the sample surface. The analysis of the separate frames allows localizing spatially the surface asperity modifications due to friction, and the number of frames defines the spatial resolution of the present method.

Random forest (RF) is a recent classification/regression technique introduced by L. Breiman [13]. It has some advantages regarding the friction problem. In particular, RF does not require any preliminary knowledge about the data distribution in the training datasets. In the present work, the input data is a statistical sequence with highly complex distributions. Involvement of the ensemble of classifiers/regressors makes the RF robust to the presence of outliers and noises, as well as makes it stable to overfitting. Considering that friction is a response of the contact between surfaces with a random configuration of asperities, it is evident that the input data are subjected to high variations, containing a lot of outliers and noise. RF is a non-parametric framework, which is adaptable to a variety of different conditions with a minimum effort. This implies its adaption to real life applications with a minimum effort.

The variation of the COF during sliding is taken as the ground truth for the estimation of the failure time. The dynamics of the COF, as shown in Fig. 4, includes three major regimes: the running-in, steady-state and scuffing. The running-in is defined as the first 50 minutes of the operating time during which the COF fluctuates extensively as the contact surfaces adjusted themselves. After the running-in, the steady-state is characterized by the fact that the mean COF is almost stable until a sharp upsurge and failure. The sharp increase in the COF of this lubricated tribo-system is called scuffing.

The prediction time interval τ was varied in multiple test-runs starting at 10 s, incrementally increased by step of 10 s, up to 310 s, when the predicted scuffing time was found to be later than the real one. Fig. 6 shows a smoothed curve of the real data (red curve) versus the predicted smoothed curves for different prediction time intervals (blues curves) of two samples. The figure includes only the prediction results of the last part of the trajectory including pre-scuffing and scuffing. This part is actually the most critical for the RF regression due to the rapid changes in the features behaviour, especially in the transition between pre-scuffing and scuffing. By scrutinizing Fig. 6, we see that the predicted and real curves are close to each other during the pre-scuffing regime. This brings confidence this regime can be forecasted up to 5 minutes before its occurrence.

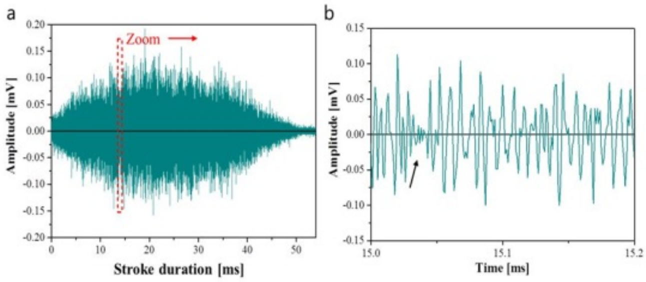

Fig. 5. (a) Typical acoustic emission (AE) signal for one stroke of the reciprocal movement and (b) zooming in of signal showing the non-stationary behavior caused by local modification of asperities.

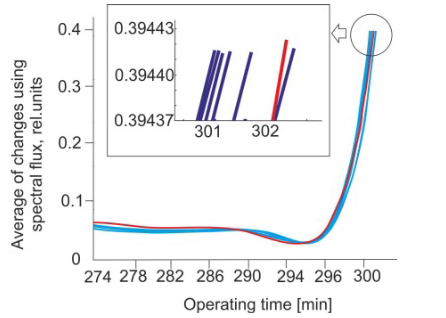

Fig. 6. The real smoothed versions of predicted data for different time intervals (blue) vs. the original data (red) for Sample 3.

2. Example: AE meets AI in the field of fracture mechanics

The example explained below was reported with details in [14]. Pre-weakening of solid materials using electric discharge is a new technique aiming at reducing the costs and energy consumption of raw materials processing in mining and recycling industries. However, the absence of an effective pre-weakening quality control prohibits its introduction into a wide practice. This work aims to present a promising solution to fulfil this gap by demonstrating the applicability of discharge pre-weakening by means of acoustic emission.

To simplify the pre-weakening quality monitoring, this study was carried out using transparent artificial samples (TAS) that allowed visual monitoring of the cracks formation induced by the electric discharge.

The TAS samples were made of poly-methyl-methacrylate (PMMA). The dielectric constant of PMMA is around 3 which fits within the range of dielectric constants of most natural solid materials that are between 3 and 20 [15].

The discharge events inside the TAS were initiated using a big scale voltage generator. The operating voltage and storage capacitance were in the range of 90 – 200 kV and 2.5 – 38 nF, respectively. The voltage exposure of the TAS was carried out in a chamber filled with water. The setup is a standard industrial environment to provoke discharge preferentially inside the solid materials in a given voltage range and it is schematically represented in Fig. 7. Such machines and process are very noisy.

All TAS were exposed to electrical pulses and the corresponding AE signals were recorded. The detection of the acoustic signals was made directly inside the water filled chamber using an acoustic hydrophone sensor R30UC. It was placed at a distance of 20 cm from the electrode gap (See Fig. 7). The AE signals were recorded with a 10 MHz sampling rate and an electrical signal amplification of 20 dB. The recording time was 16 ms and the record was synchronized with the discharge start.

In this work, we defined 3 categories and they are presented in Fig. 8. The category ***Discharge in TAS*** includes the AE that describes the pre-weakening due to the electric discharge propagation inside the TAS medium. The category ***Discharge fail*** includes partial or no discharge. The category ***Surface discharge*** contains the AE signals when the discharge occurred in the surrounding water environment or along the sample surface.

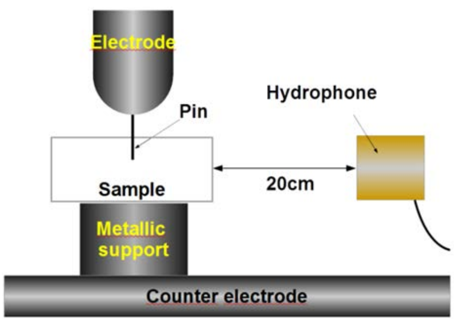

Fig. 7. Schematic view of the sample location in the discharge chamber, filled with water.

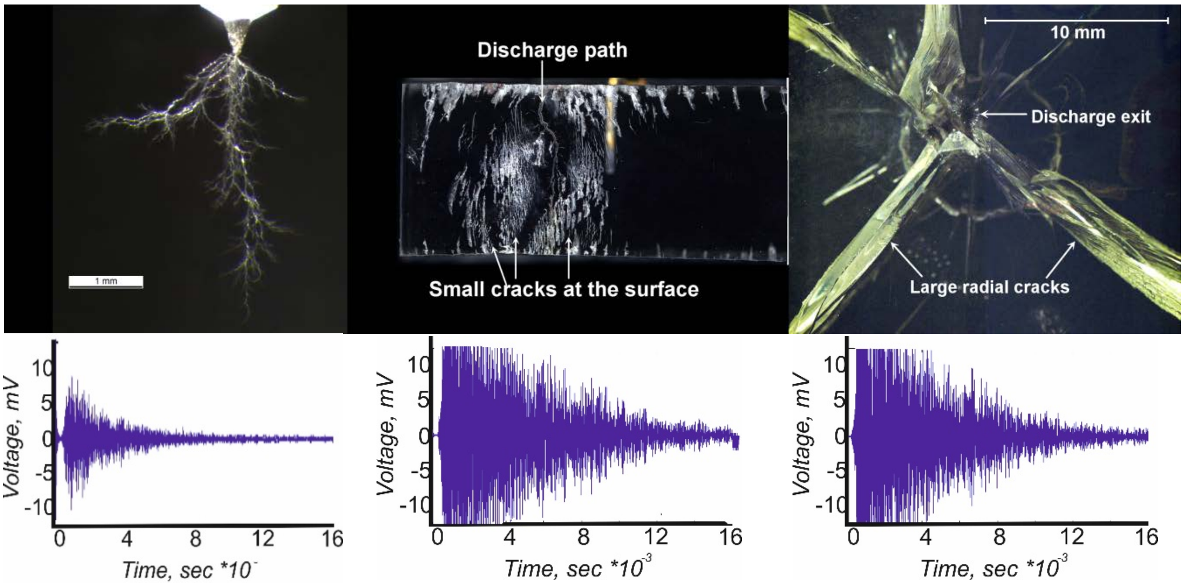

Fig. 8. Example of solid materials processed using electric discharge. A metal pin electrode is placed at the centre of the TAS. Top is an optical microscope view of TAS subjected to an electric discharge and below is its respective AE signal recorded. The figure on the left is a side view of the pin electrode area of a TAS made of PMMA for the category *Discharge fail*. The figure in the middle is a side view of a TAS made of PMMA from the category *Surface discharge*. The sample on the right is a top view of TAS made of epoxy from the category *Discharge in TAS*.

We used the method proposed by Gupta *et al.* [16] for wavelet construction for three main reasons. First, this method adapts the *M*-band wavelets to the signal in a statistical manner taking into account the diversity of the signals content. Second, it also exploits the self-similarity as a global likelihood criterion between wavelet approximation and the original signal. Finally, it supports the construction of both orthogonal and bio-orthogonal bases.

Before classification, only the most informative features are selected using the principal component analysis (PCA) [17]. The disposal of non-informative features decreases the noise in the classification and additionally reduces the computational complexity [17].
The classification was performed using support vector machine (SVM), a statistical machine learning technique proposed by Cortes and Vapnik [18].

The classification results are presented in Table 1 and, despite the noisy experiment, the event are classify with a confidence higher than 80% which is excellent. In the case of ***discharge in TAS***, no additional discharge is required. For ***discharge fail*** and ***surface discharge***, an additional discharge is required and the error with discharge in TAS is very limited having a low impact on the industrial process.

Table 1. Classification test accuracy results*

	Test results accuracy in % for:		
Ground truth reference	***Discharge in TAS***	***Discharge fail***	***Surface discharge***
Discharge in TAS	**87**	3	10
Discharge fail	7	**93**	-
Surface discharge	15	1	**84**

*Dark and light grey highlight the classification match with the ground truth and classification mistakes.

3. Example: AE meets AI in the field of laser welding or additive manufacturing

This last example presents the use of acoustic emission as a powerful tool for monitoring *in situ* and in real-time the quality of molten materials by a laser. The typical applications are laser welding or additive manufacturing.

At present, the quality control in laser welding and additive manufacturing has been diligently based on temperature or high resolution imaging of the process zone. For this, various sensors such as pyrometers, photo diodes and matrix CCD detectors are used. Unfortunately, these methods have large limitations either in temperature measurement precision or spatial resolution.

A single-mode fibre laser source StarFiber 150 P with a 1070 nm wavelength was used in this work. The laser beam went through a single-mode optical fibre with a 12 µm core diameter and focused at the surface of the sample by a focusing lens with a 170 mm focal length. This setup provides a spot size of about 30 µm diameter at the focal point ($2w_0$).

The welding trials were performed on 2 mm-thick plates of Ti_6Al_4V alloy (Grade 5) due to the ease of the microstructural characterization of the different zones such as the fusion zone, heat affected zone (HAZ) and base material.

Fig. 9 presents optical pictures (top view and cross-section) of the weld with its corresponding laser power. As seen in Fig. 9 (c), the laser illumination starts at a time of about 4 ms and lasts until 54 ms (i.e. the pulse width is 50 ms). During the process, the sample is moved with a velocity of 100 mm/s. Thus, it produces a SHADOW weld of a 5 mm length. In addition, the experiments were carried out in a controlled environment (e.g. a welding chamber filled with inert gas) to prevent any potential weld contamination such as oxidation.

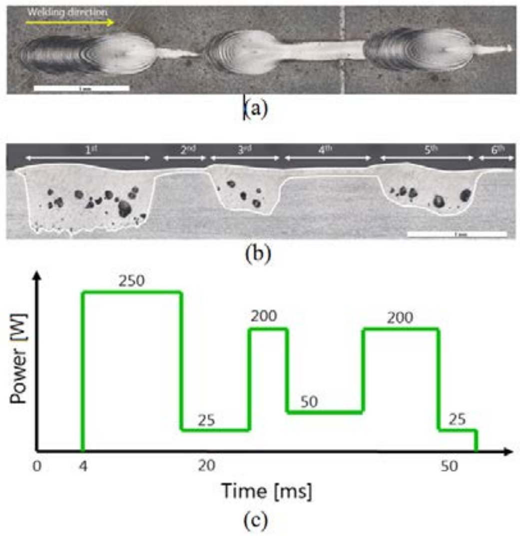

Fig. 9. Typical results of a modulated SHADOW welding on a Ti_6Al_4V alloy sample; (a) top surface, (b) longitudinal cross-section, (c) the laser pulse shape.

AE signals were recorded with a PICO sensor with frequencies between 200-750 kHz and being in contact with the work piece. The recording sampling rate was 10 MHz.

In this study, we defined four categories. ***No illumination*** is when no laser is activated. ***Conduction welding*** is for shallow welding; ***Keyhole with defects*** and ***Keyhole*** are deep penetration welds with and without defects.

In this contribution, we used a similar approach to the pre-weakening of solid materials via electrical discharge. *M*-band wavelet decomposition of recorded signals is carried out and relative energies of narrow frequency bands are taken as descriptive features. The correlation of extracted features and the real welding quality is carried out using Laplacian graph support vector machine (lapSVM) classifier [19].

Table 2. Classification test accuracy results*

	Test results accuracy in % for:			
Ground truth reference	***No illumination***	***Conduction welding***	***Keyhole***	***Keyhole with defects***
No illumination	**100**	-	-	-
Conduction welding	-	**86**	14	-
Keyhole	-	14	**80**	6
Keyhole with defects	-	-	16	**84**

*Dark and light grey highlight the classification match with the ground truth and classification mistakes.

Table 2 shows the accuracy results in the classification which is higher or equal than 90%. The less reliable results are for the category ***keyhole***. The reason is due to a transition between ***keyhole*** and ***conduction welding*** which is hard to quantify experimentally.

Conclusions

In this contribution, we presented three examples where acoustic emission meets artificial intelligence. We showed that by combining AE signals with a state-of-the-art signal processing, it is possible to address highly complex industrial processes. We demonstrated that, even in very noisy and dirty environments, we are able to achieve reliable classification of investigated events. This makes this methodology very effective for industrial applications even though it does not explains the nature of the AE signals, but this is planned as the future work.

Acknowledgements

The authors thank the Swiss Commission for Technology and Innovation (CTI- projects Nº 12358.1 PFIW-IW; 16024.1 PFEN-IW; 16697.1 PFIW-IW) for the financial support.

References

[1] C.U. Grosse and M. Ohtsu "Acoustic emission testing" Eds Springer-Verlag, 2008.
[2] V.M. Baranov, E.M. Kudryavtsev, G.A. Sarychev, V.M. Schavelin, "Acoustic emission in friction", Vol. 53. Elsevier, 2011.
[3] The Japanese Society for Non-Destructive Inspection, "Practical acoustic emission testing", Eds Springer-Verlag, 2016.
[4] B.M. Sharratt, "Non-Destructive Techniques and Technologies for Qualification of Additive Manufactured Parts and Processes: A Literature Review", Contract Report DRDC-RDDC-2015-C03
[5] D. S. Cerniglia, Michele; Pantano, Antonio; Lopatka, Rafal, "Laser Ultrasonic Technique for Laser Poweder Deposi-tion Inspection", 13th Int. Symp. Nondestructive Characterization of Materials, Le Mans, France, 2013.
[6] J. Gomes, and L. Velho, "From fourier analysis to wavelets" Vol. 3: Springer, 2015.
[7] X.Gao, R. Wang, and Y. Yang, Y. "Time-frequency Characteristics Clustering of Metallic Plume during High Power Disk Laser Welding", Proceedings of The world congress on engineering and computer science, 24-26, 2012.
[8] A.S. Sun, E. Kannatey-Asibu Jr, W.J. Williams and M. Gartner "Time-frequency analysis of laser weld signature", International Symposium on Optical Science and Technology, 103-114, 2001.
[9] I. Daubechies "Ten lectures on wavelets" Society for Industrial and Applied Mathematics, 1992.
[10] D.P. Radunovic "Wavelets: From Math to Practice" Springer Publishing Company, Incorporated, 2009.
[11] R. Polikar, "The Wavelet Tutorial", ed. Department of Electrical and Computer Engineering, Rowan University, 1996.
[12] S.A. Shevichk, F. Saeidi, B. Meylan, and K. Wasmer, "Prediction of Failure in Lubricated Surfaces Using Acoustic Time-Frequency Features and Random Forest Algorithm", IEEE Transaction on Industrial Informatics, 2016, DOI: 10.1109/TII.2016.2635082.
[13] L. Breiman, "Random forests", Machine Learning, pp. 5-32, 2001.
[14] S.A. Shevchik, B. Meylan, A. Mosaddeghi, and K. Wasmer, "Acoustic Characterization of Solid Materials Pre-weakening Using Electric Discharge", *submitted to Journal of Cleaner Production*.
[15] W.M. Telford, L.P. Geldart, and R.E. Sheriff, Applied geophysics; Cambridge university press, 2nd Edition, p.283-292, 1990.
[16] A. Gupta, S.D. Joshi, and S. Prasad, A new approach for estimation of statistically matched wavelet; IEEE transactions on signal processing, vol. 563, 5, p.1778-1793, 2005.
[17] I.T. Jolliffe, Principal Component Analysis, second edition (Springer), 2002.
[18] C. Cortes, and V. Vapnik, Support-vector networks, Machine Learning 20 (3): 273, 1995.
[19] M. Belkin, Q. Que, Z. Wang, and X. Zhou, Toward understanding complex spaces: graph Laplacians on manifolds with singularities and boundaries, JMLR workshop and conference proceedings, vol. 23, 2013.